ELSEVIER

Contents lists available at ScienceDirect

# **Chemical Physics Letters**

journal homepage: www.elsevier.com/locate/cplett



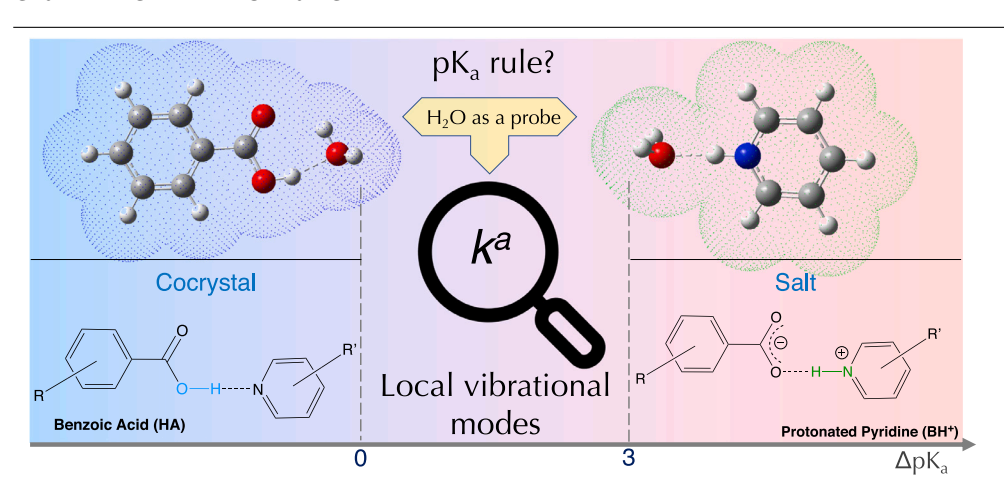
## Research paper

# The pKa rule in light of local mode force constants

Mateus Quintano<sup>a</sup>, Renaldo T. Moura Jr. <sup>a,b</sup>, Elfi Kraka <sup>a,\*</sup>

- <sup>a</sup> Computational and Theoretical Chemistry Group (CATCO), Department of Chemistry, Southern Methodist University, Dallas, TX 75275, USA
- b Department of Chemistry and Physics, Center of Agrarian Sciences, Federal University of Paraiba, Areia, PB 58397-000, Brazil

#### GRAPHICAL ABSTRACT



### HIGHLIGHTS

- Recasting the pK<sub>a</sub> rule for salts and cocrystals in terms of local mode analysis.
- · Local mode force constants were supported by the characterization of normal modes.
- A new way of inspecting cases that fall within the critical  $\Delta p K_{a}$  range of 0–3.
- Our novel assessment paves the way for crystal engineering applications.

### ARTICLE INFO

 $\begin{array}{l} \textit{Keywords:} \\ pK_a \text{ rule} \\ pK_a \text{ probe} \\ \text{The salt/cocrystal continuum} \\ \text{Local mode analysis} \end{array}$ 

## ABSTRACT

The prediction of cocrystal or molecular salt formation from organic acid and base constituents in solution usually relies on the  $pK_a$  rule, an empirical protocol based on the relative tendencies of the isolated protonated form of the base (BH<sup>+</sup>) and the isolated acid (HA) to undergo dissociation. The underlying physical rationale for this empirical rule has been missing so far. A promising step forward is to harness local mode force constants as bond strength descriptors to gain insights into the salt/cocrystal assessment. Utilizing the water  $pK_a$  probe at the  $\omega$ B97X-D(PCM)/aug-cc-pVTZ level of theory for a test set comprising various pyridine and benzoic acid derivatives, we observe a linear relationship between  $pK_a$  values and the local mode force constant  $k^a$  in this proof-of-concept study for the test examples that, according to the literature, form cocrystals or molecular salts. In addition, we propose a new way of assessing those cases where  $\Delta pK_a$  falls within the critical 0-3 range. We conclude with a future perspective on how the novel local force constant descriptor can be applied to large databases in the context of machine learning approaches.

E-mail address: ekraka@smu.edu (E. Kraka).

<sup>\*</sup> Corresponding author.

#### 1. Introduction

Cocrystals and molecular salts exhibit substantially different physicochemical properties, impacting e.g., their use in crystal engineering and/or drug design [1-6]. Therefore, it is important to predict prior to the crystallization process of a specially prepared mixture of acid and base constituents the resulting cocrystal or molecular salt character. The most common way to do this is by assessing the relative tendencies of the isolated forms, that is, the protonated form of the base (BH+) and the acid (HA), to undergo dissociation in solution. While a molecular salt is characterized by the complete proton transfer from the acid (HA) to the base (B), in a cocrystal dissociation does not occur. The identification of these two scenarios has been of recent experimental interest [7]. The components of a cocrystal usually exist in a stoichiometric ratio, and there can be more than two building blocks [1]. In other words, the salt/cocrystal assessment is mostly based on an empirical rule, the so-called  $pK_a$  rule [8–13], using differences in the acid dissociation constant ( $\Delta pK_a$ ) as guidance.  $\Delta pK_a$  is defined as follows:

$$\Delta pK_a = pK_a(BH^+) - pK_a(HA) \tag{1}$$

Typically, if  $\Delta p K_a$  is negative, the acid–base complex is predicted to yield a cocrystal. If  $\Delta p K_a$  is positive and larger than 3, the acid–base complex should result in a salt. In the  $\Delta p K_a$  range of 0–3, both cocrystal and salt formation are possible and no assertive prediction can be made. The concept is summarized in Fig. 1. Although a thermodynamic cycle approach [14] can be utilized to gain further insights into the  $p K_a$  rule, the problem of unraveling the intuitive bond strength consideration, which is concealed in Eq. (1), still remains to be addressed.

We have recently shed light on the linear relationship between the  $p\rm K_a$  and the normal vibrational frequency associated with the dissociating hydrogen of aliphatic carboxylic acids [15], which had been suggested before [16]. Nevertheless, it can be difficult to deduce intrinsic bond properties and/or assign a specific molecular fragment to a given normal vibrational mode because normal vibrational modes in large polyatomic systems are usually delocalized in collective motions of the fragments [17]. The local vibrational mode theory [18,19] originally developed by Konkoli and Cremer [20] is a powerful instrument for addressing these complications because it derives local vibrational modes and associated local mode properties from normal vibrational modes.

In this proof-of-concept study, we report for the first time local mode force constants k<sup>a</sup> from local vibrational modes [18,19] as an intrinsic bond strength descriptor of the bond associated with the dissociating hydrogen of benzoic acid and protonated pyridine test examples that are known to form cocrystals or salts (see Fig. 3), according to

Refs. [12,13]. In addition, spectator examples were included (Table 1) to guarantee a group of points with some degree of even spacing for simple linear regression between  $pK_a$  and  $k^a$ . Our target goal was to combine molecular acidity and local mode force constants, to provide a novel approach to the assessment of cocrystal/salt formation. Our methodology was designed as a means of bridging the gap between the  $pK_a$  rule and the A–H/B–H bond strength of isolated organic acids that produce cocrystals or salts when combined in solution.

#### 2. Methodology

#### 2.1. pK<sub>a</sub> Considerations

pK<sub>a</sub> values are generally reported for aqueous solution, therefore the water pK<sub>a</sub> probe approach, that is, the model chemistry involving the A–H···OH<sub>2</sub> and [B–H]<sup>+</sup> ··· OH<sub>2</sub> complexes [15], seems to be a more natural choice since for the majority of our test set the tabulated pK<sub>a</sub> values in aqueous solution at 298 K [21] were plotted against the computed local mode force constant k<sup>a</sup> values associated with A–H/B–H stretching vibrations. The simple linear regression with two-dimensional sample points served the purpose of testing the hypothesis of bond strength considerations hidden in Eq. (1) of our proof-of-concept study by linear fitting. Only for test examples 3, 14, 19, 20, 23, 25 – 27, 29, 31 – 34, 47, and 48 the pK<sub>a</sub> values from Refs. [12,13] were adopted given the lack of pK<sub>a</sub> information on these systems in Ref. [21] (see Table 1 for details).

#### 2.2. Geometry optimization and hessian matrix calculations

Electronic structure calculations at the density functional theory level were performed using the Gaussian 16 quantum chemistry program [22]. An ultra-fine grid integration and a tight convergence criterion were applied for the self-consistent field procedure. Equilibrium geometries of the pK<sub>a</sub> probe complexes, A–H···OH<sub>2</sub> and [B–H]<sup>+</sup>···OH<sub>2</sub>, as well as the subsequent Hessian matrix and its associated normal vibrational modes, were obtained employing the  $\omega$ B97X-D functional [23] and the polarizable continuum model (PCM) [24], with the default input setup utilizing water as the solvent and the radii from the Universal Force Field (UFF), in combination with Dunning's augcc-pVTZ basis set [25,26]. The reader is referred to Ref. [15] and the references therein for more information on the model chemistry that has been chosen.

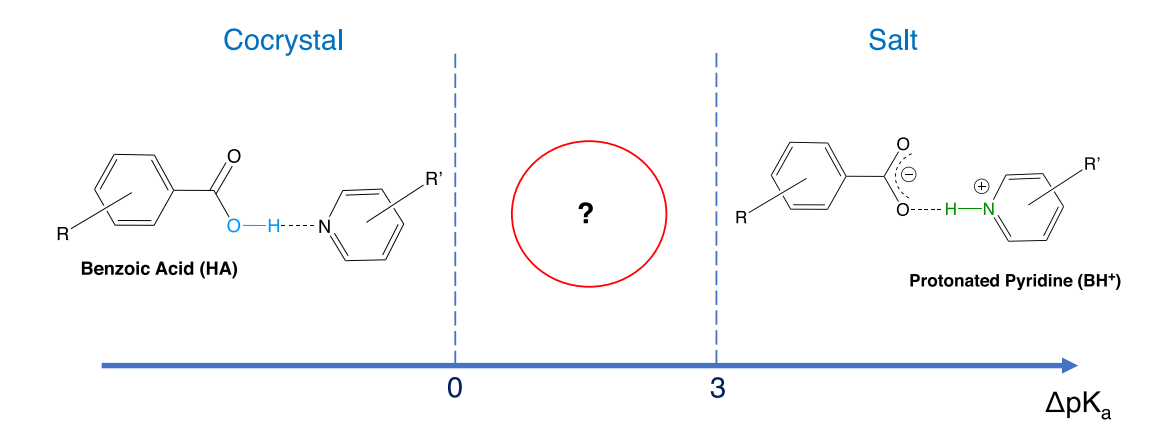


Fig. 1. Illustration of cocrystal and salt for the constituent families selected for this work within the  $\Delta p K_a$  domains predicted by the  $p K_a$  rule.

Table 1 Local mode force constant  $k^a$  in mDyn/Å associated with O–H (benzoic acid) and N–H (protonated pyridine) bonds, as well as literature (lit) and predicted (pred)  $pK_a$  values followed by their difference (Diff) for the selected test set. Unless otherwise specified, Ref. [21] is meant by literature (lit).

rei. [21] is meant by merutare (it).					
Test examples <sup>a</sup>		k <sup>a</sup>	pK <sub>a</sub> (lit)	pK <sub>a</sub> (pred) <sup>b</sup>	Diff
1	2,4-dinitrobenzoic	5.425	1.43	1.46	0.03
2	pentafluorobenzoic	5.492	1.75	1.80	0.05
3	2-chloro-4-nitrobenzoic	5.542	2.04°	2.05	0.01
4	2-nitrobenzoic	5.616	2.17	2.42	0.25
5	2-bromobenzoic	5.654	2.85	2.62	-0.23
6	2-chlorobenzoic	5.725	2.90	2.97	0.07
7	2-tert-butylbenzoic	5.813	3.54	3.42	-0.12
8	3-fluorobenzoic	5.855	3.86	3.63	-0.23
9	4-bromobenzoic	5.887	3.96	3.79	-0.17
10	4-chlorobenzoic	5.914	4.00	3.93	-0.07
11	4-fluorobenzoic	5.967	4.15	4.20	0.05
12	benzoic	5.979	4.20	4.26	0.05
13	3,5-dimethylbenzoic	6.022	4.32	4.47	0.15
14	4-methylbenzoic	6.030	4.37 <sup>d</sup>	4.52	0.15
15	4-tert-butylbenzoic	6.033	4.38	4.53	0.15
16	3,4,5-trihydroxybenzoic	6.024	4.41	4.48	0.07
17	4-methoxybenzoic	6.035	4.50	4.54	0.04
18	4-phenoxybenzoic	6.040	4.57	4.57	0.00
19	4-hydroxybenzoic	6.034	4.57 <sup>d</sup>	4.54	-0.03
20	4-aminobenzoic	6.055	4.86 <sup>d</sup>	4.64	-0.22
21	2-fluoropyridine	4.622	-0.44	0.06	0.50
22	2-chloropyridine	4.701	0.49	0.69	0.20
23	2-bromopyridine	4.740	0.79 <sup>c</sup>	1.00	0.21
24	4-nitropyridine	4.768	1.61	1.22	-0.39
25	3-amino-2-bromopyridine	4.854	1.72 <sup>c</sup>	1.91	0.19
26	4-cyanopyridine	4.830	1.92 <sup>d</sup>	1.72	-0.20
27	3-amino-2-chloropyridine	4.816	2.42 <sup>c</sup>		
28	3-chloropyridine	4.905	2.81	2.31	-0.50
29	2-amino-5-nitropyridine	5.393	2.82 <sup>c</sup>		
30	4-chloropyridine	5.056	3.83	3.52	-0.31
31	2-amino-3-bromopyridine	5.798	4.14 <sup>c</sup>		
32	2-chloro-3-hydroxypyridine	4.725	4.32 <sup>c</sup>		
33	2-amino-5-bromopyridine	5.834	4.65 <sup>c</sup>		
34	2-amino-5-chloropyridine	5.732	4.67 <sup>c</sup>		
35	3-methoxypyridine	5.151	4.78	4.28	-0.50
36	pyridine	5.247	5.23	5.04	-0.19
37	3-methylpyridine	5.280	5.70	5.30	-0.40
38	4-methylpyridine	5.415	5.99	6.38	0.39
39	2-methylpyridine	5.424	6.00	6.45	0.45
40	3,5-dimethylpyridine	5.391	6.15	6.19	0.04
41	2,5-dimethylpyridine	5.447	6.40	6.64	0.24
42	3,4-dimethylpyridine	5.437	6.46	6.56	0.10
43	2,3-dimethylpyridine	5.497	6.57	7.04	0.47
44	2,6-dimethylpyridine	5.487	6.65	6.96	0.31
45	2,4-dimethylpyridine	5.529	6.99	7.29	0.30
46	2,4,6-trimethylpyridine	5.546	7.43	7.43	0.00
47	4-aminopyridine	5.715	9.26 <sup>d</sup>	8.77	-0.49
48	4-N,N-dimethylaminopyridine	5.759	9.52 <sup>d</sup>	9.12	-0.40
	. , , , ,				

 $^{\rm a}\mbox{`acid'}$  was omitted from the names of the benzoic acids  $1\mbox{--}20$  to avoid redundancy.

## 2.3. Local mode analysis

The delocalization conundrum of normal vibrational modes [17] can be resolved by the local vibrational mode theory [18,19], whose foundations were laid by Konkoli and Cremer [20]. The cornerstone of the theory is to extract local vibrational modes including intrinsic bond properties from normal vibrational modes. Zou and Cremer demonstrated that the local mode force constant  $k^a$  is a local descriptor of the intrinsic strength of the bond or interaction between two atoms under consideration [27]. The local vibrational mode theory also offers a unique way to analyze vibrational spectra via the decomposition of a given normal vibrational mode into local mode components, the so-called CNM procedure [28,29], which is physically based on

an important one-to-one relationship between a complete set of non-redundant local modes and their normal mode counterparts via an adiabatic connection scheme [30].

All the subtleties of local mode analysis have been recently discussed in two comprehensive feature articles [18,19]. Hence, only a few key aspects of the method are described in the following. The normal vibrational modes  $\mathbf{d}_n$  (in internal coordinates) and the diagonal force constant matrix  $\mathbf{K}$  (in normal coordinates) can be used to determine local mode vectors  $\mathbf{a}_n$  associated with the internal coordinates  $q_n$ , as demonstrated by Konkoli and Cremer:

$$\mathbf{a}_n = \frac{\mathbf{K}^{-1} \mathbf{d}_n^{\dagger}}{\mathbf{d}_n \mathbf{K}^{-1} \mathbf{d}_n^{\dagger}} \tag{2}$$

It should be pointed out that  $\mathbf{d}_n$  and  $\mathbf{K}$  can be easily obtained from standard quantum chemistry packages after a vibrational frequency calculation. The local mode force constant  $k_n^a$  can be calculated as shown below

$$k_n^a = \mathbf{a}_n^{\dagger} \mathbf{K} \mathbf{a}_n = (\mathbf{d}_n \mathbf{K}^{-1} \mathbf{d}_n^{\dagger})^{-1}$$
(3)

Every normal vibrational mode (associated with absorption peaks) can be broken down into local vibrational mode percentage contributions from a non-redundant set of local vibrational modes using the CNM procedure, which is an integral part of local mode analysis. The overlapping encoded by  $S_{nu}$  [18,31] is defined by

$$S_{n\mu} = \frac{\langle \mathbf{a}_n^{\mathbf{x}} | \mathbf{F}^{\mathbf{x}} | \mathbf{l}_{\mu} \rangle^2}{\langle \mathbf{a}_n^{\mathbf{x}} | \mathbf{F}^{\mathbf{x}} | \mathbf{a}_n^{\mathbf{x}} \rangle \langle \mathbf{l}_{\mu} | \mathbf{F}^{\mathbf{x}} | \mathbf{l}_{\mu} \rangle}$$
(4)

with  $\mathbf{a}_n^{\mathbf{x}}$ ,  $\mathbf{F}^{\mathbf{x}}$  and  $\mathbf{l}_{\mu}$  being the local vibrational mode, the Hessian matrix and the normal vibrational mode in Cartesian coordinates. The percentage contribution  $C_{n\mu}^{\%}$  (local mode contribution) of the local vibrational mode  $\mathbf{a}_n^{\mathbf{x}}$  to the normal vibrational mode  $\mathbf{l}_{\mu}$  is then calculated as follows [31]

$$C_{n\mu}^{\%} = \frac{S_{n\mu}}{\sum_{m}^{N_{vib}} S_{m\mu}} 100 \tag{5}$$

The local mode theory has advanced over the past years as a powerful bond strength descriptor accounting for both covalent bonds and non-covalent interactions stretching from hydrogen bonds, halogen bonds to tetrel bonds and  $\pi$ -whole interactions. A comprehensive collection of examples can be found in Refs. [18,19], some recent examples include Refs. [32,33]. Different molecular environments were considered such as systems in solution [34] or in proteins [35]. A whole new scope of chemical systems were unlocked with the extension of the local mode theory to periodic systems and crystals [36,37]. Recently, a novel explanation of the inverse connection between the lanthanide-ligand strength and ligand effective polarizability has been provided by the incorporation of local mode force constants into lanthanide spectroscopy, shedding light on bonding in the realm of lanthanide chemistry [38].

The automatic generation of the non-redundant and complete sets of local vibrational modes were obtained for test examples 1-48 (see Table 1) using our new LModeAGen protocol [39] and the corresponding local mode analysis was performed with the standalone LModeA package [40]. The aim was to show CNM as an assessment tool for the local character of the normal O–H/N–H stretching vibration in compounds 1-48. Our test set also contains spectator examples (those in Table 1 other than what Fig. 3 shows) that served the purpose of providing a somewhat evenly spaced collection of points for linear fitting with one independent variable ( $k^a$ ) and one dependent variable ( $pK_a$ ).

#### 3. Results and discussion

Fig. 2 summarizes the CNM results by displaying for each of the 20 benzoic acids and 28 protonated pyridines from Table 1 the % of local

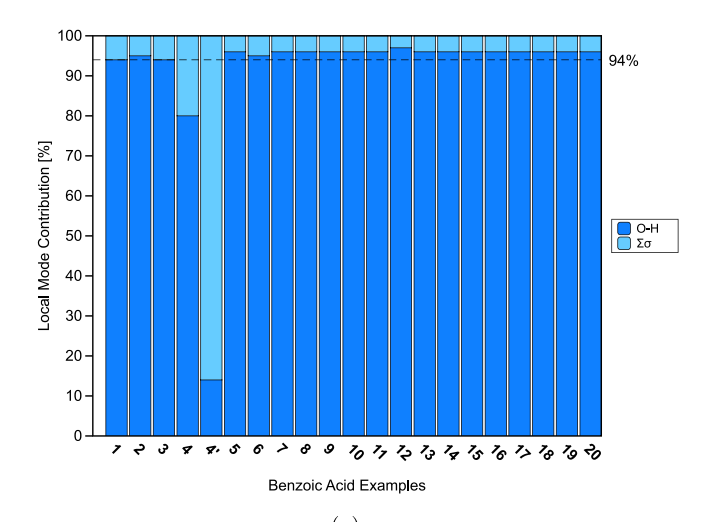
<sup>&</sup>lt;sup>b</sup>Benzoic acids:  $pK_a$  (pred) = -25.9525 + 5.05267 k<sup>a</sup> (O-H)

Pyridines:  $pK_a$  (pred) = -36.8057 + 7.97542 k<sup>a</sup> (N-H), without outliers.

<sup>&</sup>lt;sup>c</sup>Ref. [12].

<sup>&</sup>lt;sup>d</sup>Ref. [13].

4.59



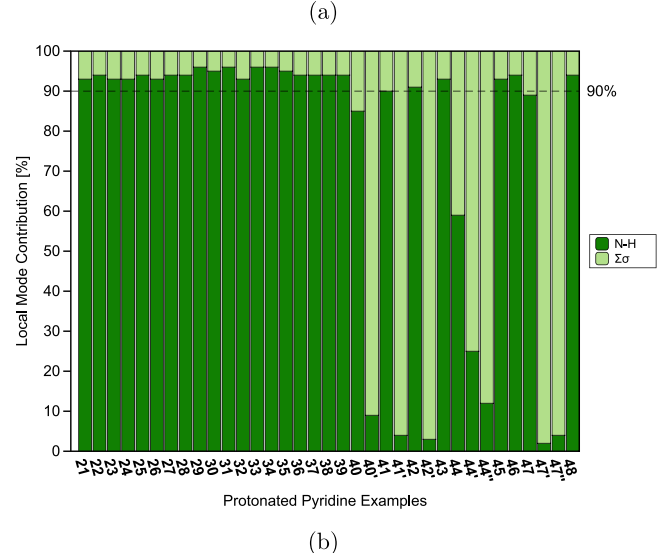


Fig. 2. CNM plot of the normal vibrational mode associated with the O–H and N–H stretching vibrations for (a) benzoic acid examples and (b) protonated pyridine examples, respectively. Secondary normal vibrational modes with appreciable O–H/N–H character are denoted by ' and ". Calculations for the model chemistry utilizing the water pK<sub>a</sub> probe at the  $\omega$ B97X-D(PCM)/aug-cc-pVTZ level of theory.  $\Sigma\sigma$  comprises the summation of all the unrelated  $\sigma$  local mode contributions.

O-H and N-H stretching mode character, respectively. As shown in Fig. 2a, the normal modes associated with the O-H stretching vibrations are more than 94% localized. However, 2-nitrobenzoic acid 4 is an exception, with two normal vibrational modes that together make the local O-H stretching mode character of 94%. For the protonated pyridine examples, Fig. 2b reveals a worse delocalization scenario. The normal vibrational modes associated with the N-H stretching vibrations are more or less above a localization of 90%. However, 3,5dimethylpyridine 40, 2,5-dimethylpyridine 41, 3,4-dimethylpyridine 42, 2,6-dimethylpyridine 44, and 4-aminopyridine 47 are exceptions. Since a sound bond strength descriptor is demanded to shed light on Eq. (1), such a recurring delocalization of the normal vibrational modes associated with the O-H and N-H stretching vibrations via CNM makes a convincing case for the utilization of ka to gauge the intrinsic strength of the O-H and N-H bonds for the isolated benzoic acid and protonated pyridine test examples, respectively.

The investigation of the relationship between  $pK_a$  values and local mode force constants  $k^a$  in this proof-of-concept study showcases the

Table 2  $ΔpK_a$  (pred) values following pairwise combinations of the test examples that form cocrystals or salts according to the literature [12,13]. Calculations for the model chemistry utilizing the water  $pK_a$  probe at the ωB97X-D(PCM)/aug-cc-pVTZ level

3† 12 14 17 19 20 BH<sup>+</sup> 23 -1.05 25 -0.14-2.54 -2.80 -2.82 -2.82 -2.93 26 27 29 31 32 33 34 4.91 44 47 4.52 4.26 4.23 4.24 4.13

4.61

4 87

48

test examples, as represented in Fig. 3 and rendered with different colors in Fig. 4, that form cocrystals or molecular salts [12,13]. We found a significant linear correlation between pK $_{\rm a}$  and k $^{\rm a}$  (R $^{\rm 2}=0.9832$ ) for the 20 benzoic acids 1–20 investigated in this work, as depicted in Fig. 4a.

As shown in Table 1, the linear regression takes the form of pK<sub>a</sub> (pred) =  $-25.9525 + 5.05267 \, k^a \, (O-H)$ . Fig. 4b shows that for the protonated pyridines there is also a significant linear correlation between pK<sub>a</sub> and k<sup>a</sup> (R<sup>2</sup>=0.9846), but test examples **27**, **29**, **31**, **32**, **33**, and **34** occur as outliers and, therefore were omitted from the linear regression pK<sub>a</sub> (pred) =  $-36.8057 + 7.97542 \, k^a \, (N-H)$  also given in Table 1. These outliers are not a mere coincidence (see Table 2). On the whole, the predicted pK<sub>a</sub> values exhibit a satisfactory agreement with the literature data, with differences between experimental and predicted pK<sub>a</sub> values being smaller than 0.5 pK<sub>a</sub> units. Hence, one can tell quite plainly that Fig. 4 provides an elucidation of the bond strength aspect which is implicit in the pK<sub>a</sub> rule.

In that sense, for the systems that follow the linear relationships in Fig. 4 and Table 1, Eq. (1) can be rewritten as

$$\Delta pK_a = a k^a (BH^+) - b k^a (HA) + c$$
(6)

where a, b, and c are anticipated to be environment- and family-dependent coefficients. Eq. (6) contributes to a better understanding of cocrystal/salt formation in that it furnishes a theoretical basis for how local mode force constants associated with O–H/N–H stretching vibrations can be combined to give  $\Delta p K_a$ , thereby substantiating theoretically why the  $p K_a$  rule works. Table 2 collects  $\Delta p K_a$  (pred) values following pairwise combinations of the test examples that form cocrystals or salts according to the literature [12,13].

The pairs in the first column form cocrystals and salts as reported in Ref. [13], but question marks (?) indicate the pairs containing the protonated pyridine examples that are outliers in the "pK $_{\rm a}$  (lit) versus k $^{\rm a}$  (N–H)" relationship shown in Fig. 4b. All the remaining entries form salts or cocrystals outside the intermediate region in close agreement with the pK $_{\rm a}$  rule as reported in Ref. [12].

The pairs **27:3**, **29:3**, **31:3**, **32:3**, **33:3**, and **34:3** fall within the  $\Delta p K_a$  (lit) range of 0–3 [13] and exhibit a  $k^a$  (N–H)/ $k^a$  (O–H) ratio of 0.869, 0.973, 1.046, 0.853, 1.053, and 1.034, respectively. Such ratio values show the relative strengths of N–H and O–H bonds and therefore suggest the formation of cocrystal (**27:3**), cocrystal (**29:3**), salt (**31:3**), cocrystal (**32:3**), salt (**33:3**), and salt (**34:3**), respectively; i.e., stronger N–H bonds suggest the formation of salt while stronger O–H bonds suggest the formation of cocrystal. Our prediction happens

 $<sup>^\</sup>dagger$  All the pairwise combinations in this column are from Ref. [13]. The pairwise combinations elsewhere are from Ref. [12]. Question marks (?) indicate the pairs containing the protonated pyridine examples that are outliers in the "pKa (lit) versus  $k^a$  (N–H)" relationship shown in Fig. 4b.

Fig. 3. Examples from the test set that form cocrystals or salts, according to the literature [12,13], are represented schematically. The corresponding  $k^a$  value in mDyn/Å for the model chemistry utilizing the water pK<sub>a</sub> probe at the  $\omega$ B97X-D(PCM)/aug-cc-pVTZ level of theory is given below each structure along with the numbering from Table 1.

to be in remarkable agreement with the literature [13] and offers for the selected test set a novel assessment of the intermediate region of  $\Delta p K_a$  which is known as the salt/cocrystal continuum [9]. All the reported discoveries are expected to furnish an explanation of the pKa rule in terms of a vibrational spectroscopy property, that is, on a physical basis. In addition, this report of the local mode force constant ka as a local descriptor herein discussed for the first time can be extended for large datasets in the context of machine learning approaches aimed at comprehensive pKa estimates stretching beyond the realm of crystal engineering. Interestingly, in an effort to increase the effectiveness of cocrystal screening, the number of coformers that must be tested empirically has recently been reduced using the pK<sub>a</sub> rule in combination with predictions made by an artificial neural network model [41]. In passing, work is in progress in our group towards pK<sub>a</sub> prediction utilizing an extensive model [42] containing k<sup>a</sup> as sound local descriptors. Such pK<sub>a</sub> prediction is expected to promote the advancement of drug design characterizations and will include biologically relevant systems. Furthermore, the local force constants could also turn out to be a valuable descriptor in a large database for machine learning techniques.

## 4. Conclusion

We have devised a novel protocol for predicting cocrystals and salts in solution based on the local mode analysis. We have recast the pK<sub>a</sub> rule in terms of the local mode force constant ka for the cocrystal/salt components in solution by devising a methodology utilizing the water pK<sub>a</sub> probe at the ωB97X-D(PCM)/aug-cc-pVTZ level of theory. Our formulation opens the gates to a novel interpretation based on the local vibrational mode theory and offers a new protocol of identification. Among test examples 1 - 48, anomalous behavior arises from the pyridines 27, 29, 31, 32, 33, and 34, which do not obey the linear relationship between pKa (predicted) and ka (N-H) and happen to give rise to complexes in the ΔpK<sub>a</sub> range of 0-3, the salt/cocrystal continuum. For the pairwise combinations containing the pyridine outliers, a different regime takes place, namely, that of local mode force constant ratios as a means to probe the relative strengths of N-H and O-H bonds, consequently predicting for the first time the formation of cocrystal or salt within the intermediate region of  $\Delta pK_a$ . We hope that our novel assessment will find its entrance into the crystal engineering and drug design communities utilizing our protocol as a guidance for designing

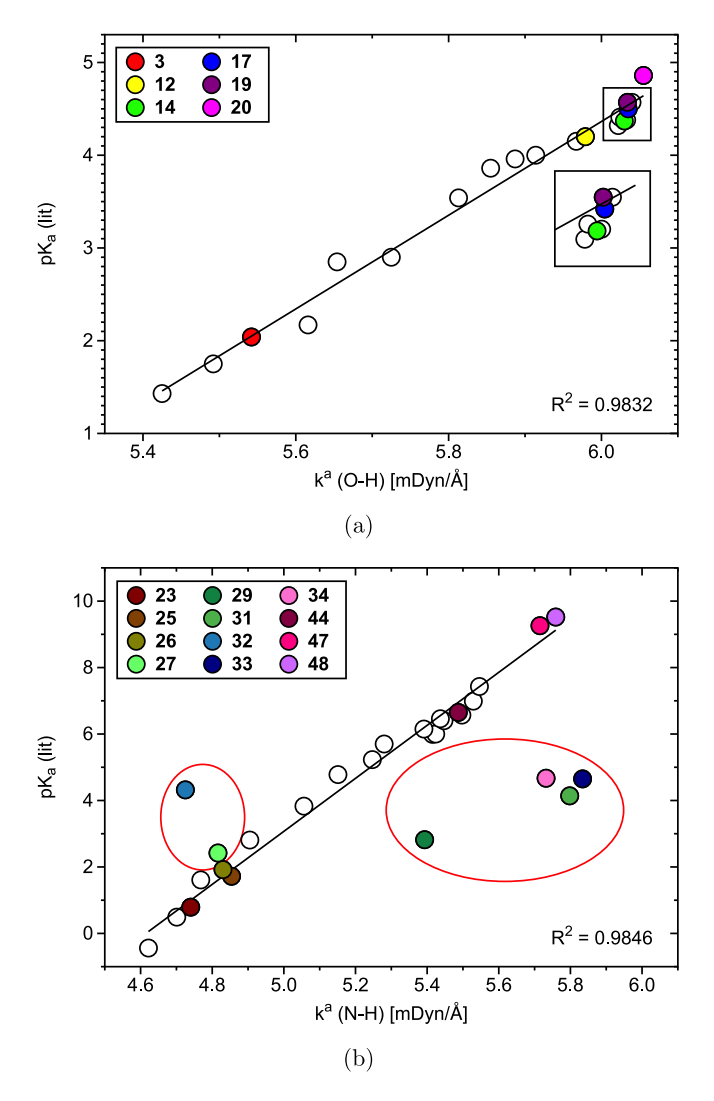


Fig. 4. Relationship between  $pK_a$  values and local mode force constants  $k^a$  for (a) benzoic acid examples and (b) protonated pyridine examples. Results for the model chemistry utilizing the water  $pK_a$  probe at the  $\omega B97X-D(PCM)/aug-cc-pVTZ$  level of theory.

compounds with a specific cocrystal and/or salt character, and that our protocol will replace over time the empirical  $pK_a$  rule.

#### CRediT authorship contribution statement

Mateus Quintano: Conceptualization, Execution, Visualization, First draft writing. Renaldo T. Moura Jr.: Conceptualization, Execution, Editing. Elfi Kraka: Conceptualization, Evaluation, Editing, Supervision.

# Declaration of competing interest

The authors declare the following financial interests/personal relationships which may be considered as potential competing interests: Elf Kraka reports was provided by Southern Methodist University. Elf Kraka reports a relationship with Southern Methodist University that includes: employment. There are no additional relationships or activities to declare.

#### Acknowledgments

We thank SMU's Center for Research Computing for providing generous computational resources. M. Q. thanks SMU for the Computational Science and Engineering Fellowship. We also thank Ayesh

Madushanka for his comments of great value. This work was financially supported by the United States National Science Foundation, Grant CHE 2102461.

#### References

- C.B. Aakeröy, M.E. Fasulo, J. Desper, Cocrystal or salt: Does it really matter? Mol. Pharmacol. 4 (2007) 317–322.
- [2] E. Pindelska, A. Sokal, W. Kolodziejski, Pharmaceutical cocrystals, salts and polymorphs: Advanced characterization techniques, Adv. Drug Deliv. Rev. 117 (2017) 111–146.
- [3] C. Zhang, Y. Xiong, F. Jiao, M. Wang, H. Li, Redefining the term of Cocrystal and broadening its intention, Cryst. Growth Des. 19 (2019) 1471–1478.
- [4] N.K. Duggirala, S.M. LaCasse, M.J. Zaworotko, J.F. Krzyzaniak, K.K. Arora, Pharmaceutical cocrystals: Formulation approaches to develop robust drug products, Cryst. Growth Des. 20 (2020) 617–626.
- [5] G. Bolla, B. Sarma, A.K. Nangia, Crystal engineering of pharmaceutical cocrystals in the discovery and development of improved drugs, Chem. Rev. 122 (2022) 11514–11603.
- [6] A.V.S.D. Surampudi, S. Ramakrishna, A. Pallavi, S. Balasubramanian, Novel salts and cocrystals of the antifolate drug trimethoprim and their role in the enhancement of solubility and dissolution, CrystEngComm 25 (2023) 1220–1231.
- [7] S. Tothadi, T.R. Shaikh, S. Gupta, R. Dandela, C.P. Vinod, A.K. Nangia, Can we identify the salt-cocrystal continuum state using XPS? Cryst. Growth Des. 21 (2021) 735–747.
- [8] B.R. Bhogala, S. Basavoju, A. Nangia, Tape and layer structures in cocrystals of some di-and tricarboxylic acids with 4, 4'-bipyridines and isonicotinamide. From binary to ternary cocrystals, CrystEngComm 7 (2005) 551–562.
- [9] S.L. Childs, G.P. Stahly, A. Park, The salt-cocrystal continuum: The influence of crystal structure on ionization state, Mol. Pharmacol. 4 (2007) 323–338.
- [10] S. Mohamed, D.A. Tocher, M. Vickers, P.G. Karamertzanis, S.L. Price, Salt or cocrystal? A new series of crystal structures formed from simple pyridines and carboxylic acids, Cryst. Growth Des. 9 (2009) 2881–2889.
- [11] A.J. Cruz-Cabeza, Acid-base crystalline complexes and the pKa rule, CrystEngComm 14 (2012) 6362–6365.
- [12] A. Mukherjee, G.R. Desiraju, Combinatorial exploration of the structural landscape of acid-pyridine cocrystals. Cryst. Growth Des. 14 (2014) 1375–1385.
- [13] A. Lemmerer, S. Govindraju, M. Johnston, X. Motloung, K.L. Savig, Co-crystals and molecular salts of carboxylic acid/pyridine complexes: can calculated pKa's predict proton transfer? A case study of nine complexes, CrystEngComm 17 (2015) 3591–3595.
- [14] A.J. Cruz-Cabeza, M. Lusi, H.P. Wheatcroft, A.D. Bond, The role of solvation in proton transfer reactions: implications for predicting salt/co-crystal formation using the △pK<sub>a</sub> rule, Faraday Discuss. 235 (2022) 446–466.
- [15] M. Quintano, E. Kraka, Theoretical insights into the linear relationship between  $pK_u$  values and vibrational frequencies, Chem. Phys. Lett. 803 (2022) 139746–1–139746–7.
- [16] L. Tao, J. Han, F.-M. Tao, Correlations and predictions of carboxylic acid pK<sub>a</sub> values using intermolecular structure and properties of hydrogen-bonded complexes, J. Phys. Chem. A 112 (2008) 775–782.
- [17] E.B. Wilson, Some mathematical methods for the study of molecular vibrations, J. Chem. Phys. 9 (1941) 76–84.
- [18] E. Kraka, M. Quintano, H.W.L. Force, J.J. Antonio, M. Freindorf, The local vibrational mode theory and its place in the vibrational spectroscopy arena, J. Phys. Chem. A 126 (2022) 8781–8900.
- [19] E. Kraka, W. Zou, Y. Tao, Decoding chemical information from vibrational spectroscopy data: Local vibrational mode theory, WIREs: Comput. Mol. Sci. 10 (2020) 1480.
- [20] Z. Konkoli, D. Cremer, A new way of analyzing vibrational spectra, I. Derivation of adiabatic internal modes, Int. J. Quantum Chem. 67 (1998) 1–9.
- [21] W.M. Haynes, D.R. Lide, T.J. Bruno, CRC HandBook of Chemistry and Physics, 97th ed., CRC Press, 2016-2017.
- [22] M.J. Frisch, G.W. Trucks, H.B. Schlegel, G.E. Scuseria, M.A. Robb, J.R. Cheeseman, G. Scalmani, V. Barone, G.A. Petersson, H. Nakatsuji, et al., Gaussian 16 Revision C.01, gaussian Inc., Wallingford CT, 2016.
- [23] J.-D. Chai, M. Head-Gordon, Long-range corrected hybrid density functionals with damped atom-atom dispersion corrections, Phys. Chem. Chem. Phys. 10 (2008) 6615–6620.
- [24] J. Tomasi, B. Mennucci, R. Cammi, Quantum mechanical continuum solvation models, Chem. Rev. 105 (2005) 2999–3094.
- [25] T.H. Dunning, Gaussian basis sets for use in correlated molecular calculations, I. The atoms boron through neon and hydrogen, J. Chem. Phys. 90 (1989) 1007–1023
- [26] R.A. Kendall, T.H. Dunning, R.J. Harrison, Electron affinities of the first-row atoms revisited, systematic basis sets and wave functions, J. Chem. Phys. 96 (1992) 6796–6806.

- [27] W. Zou, D. Cremer, C<sub>2</sub> in a box: Determining its intrinsic bond strength for the X<sup>1</sup> Σ<sup>+</sup><sub>\*</sub> ground state, Chem. Eur. J. 22 (2016) 4087–4097.
- [28] N. verma, Y. Tao, W. Zou, X. Chen, X. Chen, M. Freindorf, E. Kraka, A critical evaluation of vibrational stark effect (VSE) probes with the local vibrational mode theory, Sensors 20 (2020) 2358.
- [29] M. Quintano, A.A.A. Delgado, R.T. Moura Jr., M. Freindorf, E. Kraka, Local mode analysis of characteristic vibrational coupling in nucleobases and Watson-Crick base pairs of DNA, Electron. Struct. 4 (12) (2022) 044005-1- 044005-17.
- [30] W. Zou, R. Kalescky, E. Kraka, D. Cremer, Relating normal vibrational modes to local vibrational modes with the help of an adiabatic connection scheme, J. Chem. Phys. 137 (2012) 084114.
- [31] Z. Konkoli, D. Cremer, A new way of analyzing vibrational spectra, Int. J. Quantum Chem. 67 (1998) 29–40.
- [32] M. Freindorf, M. McCutcheon, N. Beiranvand, E. Kraka, Dihydrogen bondingseen through the eyes of vibrational spectroscopy, Molecules 28 (2023) 263–1–263–23.
- [33] W. Zou, M. Freindorf, V. Oliveira, Y. Tao, E. Kraka, Weak and strong π interactions between two monomers assessed with local vibrational mode theory, Can. J. Chem. (2023) http://dx.doi.org/10.1139/cjc--2022--0254.
- [34] A.A.A. Delgado, D. Sethio, I. Munar, V. Aviyente, E. Kraka, Local vibrational mode analysis of ion-solvent and solvent-solvent interactions for hydrated Ca<sup>2</sup>+ clusters, J. Chem. Phys. 153 (2020) 224303–1–224303–11.
- [35] M. Freindorf, E. Kraka, Critical assessment of the FeC and CO bond strength in carboxymyoglobin - A QM/MM local vibrational mode study, J. Mol. Model. 26 (2020) 281–1–281–15.

- [36] Y. Tao, W. Zou, D. Sethio, N. Verma, Y. Qiu, C. Tian, D. Cremer, E. Kraka, In situ measure of intrinsic bond strength in crystalline structures: Local vibrational mode theory for periodic systems, J. Chem. Theory Comput. 15 (2019) 1761–1776.
- [37] S. Nanayakkara, Y. Tao, E. Kraka, Capturing individual hydrogen bond strengths in ices via periodic local vibrational mode theory: Beyond the lattice energy picture, J. Chem. Theory Comput. 18 (2022) 562–579.
- [38] R.T. Moura, M. Quintano, C.V. Santos Jr., V.A. Albuquerque, E.C. Aguiar, E. Kraka, A.N. Carneiro Neto, Featuring a new computational protocol for the estimation of intensity and overall quantum yield in lanthanide chelates with applications to Eu(III) mercapto-triazole schiff base ligands, Opt. Mater. X 16 (2022) 100216–1–100216–15.
- [39] R.T.J. Moura, M. Quintano, J.J. Antonio, M. Freindorf, E. Kraka, Automatic generation of local vibrational mode parameters: From small to large molecules and OM/MM systems, J. Phys. Chem. A 126 (2022) 9313–9331.
- [40] W. Zou, Y. Tao, M. Freindorf, M.Z. Makoś, N. Verma, D. Cremer, E. Kraka, Local Vibrational Mode Analysis (Imodea, Computational and Theoretical Chemistry Group (CATCO), Southern Methodist University, Dallas, TX, USA, 2022.
- [41] P. Kim, I.-S. Lee, J.-Y. Kim, M.E. Mswahili, Y.-S. Jeong, W.-J. Yoon, H.-S. Yun, M.-J. Lee, G.J. Choi, A study to discover novel pharmaceutical cocrystals of pelubiprofen with a machine learning approach compared, CrystEngComm 24 (2022) 3938–3952.
- [42] R.T. Madushanka, A. Moura Jr., E. Verma, N. Kraka, Quantum mechanical assessment of protein-ligand hydrogen bond strength patterns: Insights from semiempirical tight-binding and local vibrational mode theory, Int. J. Mol. Sci. 24 (2023) 6311-1-6311-24.